Low-Frequency Raman Spectra of Nitric Acid Hydrates

Hinrich Grothe,*,† Cathrine E. Lund Myhre,‡ and Claus J. Nielsen‡

Institute of Materials Chemistry, Vienna University of Technology, Veterinärplatz 1/GA, A-1210 Vienna, Austria, and Department of Chemistry, University of Oslo, P.O. Box 1033 Blindern, N-0372 Oslo, Norway

Received: September 28, 2005; In Final Form: October 31, 2005

Raman spectra of solid nitric acid hydrates (NAM, α- and β-NAD, α- and β-NAT, and NAP) are obtained in the low-frequency region 20−175 cm^{-1} where phonon bands show characteristic patterns. This fingerprint information, intimately related to the structure and symmetry of the unit cell, is well suited for observation of phase changes in solid nitric acid hydrates and allows the distinction of mixtures of different hydrate phases. The low-frequency spectra are correlated with the spectra of the respective symmetric NO stretching vibration (1000−1080 cm^{-1}), with literature data, and with X-ray diffraction patterns.

1. Introduction

More than 110 years ago, Pickering identified the first nitric acid hydrate phases by thermal analysis.[1] Sixty years later, Luzzati determined the crystal structures of the thermodynamically stable phases nitric acid monohydrate (NAM) and nitric acid trihydrate (NAT) by X-ray diffraction.[2,3] Herzog-Cance et al. published the first Raman spectra of these hydrates.[4,5] The interest in nitric acid hydrates had a renaissance with the discovery of the so-called ozone hole over the Antarctic polar region. Nitric acid and water had been identified as major constituents of Polar Stratospheric Clouds (PSC) which assist in transforming inactive reservoir compounds (e.g., HCl and $ClONO_2$) into active chlorine species (e.g., HOCl, Cl_2, etc.) forcing the ozone depletion.[6] It is currently debated which of the nitric acid hydrate phases might persist under the extreme conditions of the polar stratosphere.[7−11] In this context, it should be noted that the PSC particles are essentially not in thermodynamic equilibrium with their environment. Therefore, particular attention should be paid not only to the equilibrium phases but also to the nonequilibrium modifications: their metastable existence in the stratosphere should not a priori be neglected. Particularly, the nitric acid dihydrate (NAD) is of interest due to its outstanding nucleation properties.[12−14]

For an unambiguous phase assignment of solid hydrates, a diffraction technique is often the method of choice. However, most studies applied to the properties of nitric acid hydrates so far have been carried out by infrared (IR) and Raman spectroscopy,[11,15−23] and it is therefore important to correlate the spectra and the diffraction patterns. This task is hampered by the insufficient sensitivity of the molecular vibrations with respect to solid-phase changes — vibrational spectroscopy probes only the short-range order, that is, the direct environment of the ions and molecules (NO_3^-, H_2O, H_3O^+, $H_5O_2^+$, or $H_7O_3^+$) in question. The most intense Raman and IR bands of these species are located in the NO (1000−1450 cm^{-1}) and OH stretching (3300−3500 cm^{-1}) regions, and while following a phase change these bands exhibit only minor intensity variations and frequency shifts. In a few cases, a split of these bands due to changes in the site symmetry of the respective crystal occurs.[15,24] In a recent work, we have differentiated a low- and a high-temperature modification of NAD by XRD, FTIR, and Raman spectroscopy, paying particular attention to the low-frequency region (20−200 cm^{-1}).[25,26] LeBrun et al.[27] have used the same techniques giving survey spectra in the mid-IR frequency region (400−3600 cm^{-1}). A comparison shows that the phonon bands located in the low-frequency region are better suited to distinguish between crystal lattices exhibiting slightly different structures. Therefore, in the present work a Raman analysis of the low-frequency region of all nitric acid hydrates known to date is presented and correlated with the respective symmetric NO stretching vibration band in the mid-frequency region.

2. Experimental Section

We have recently described the details of a quenching technique, which enables us to generate solid amorphous samples of well-defined stoichiometry.[25,26] From these nonequilibrium samples we have grown the essentially pure hydrate phases — stable as well as metastable. The preparation procedure has been verified by the aid of XRD, which assured the phase composition. In the case of Raman spectroscopy we have even simplified this quenching method by plunging a glass tube with the respective nitric acid solutions (298 K) in a liquid nitrogen bath (77 K). The tube has a small capillary extension (outer diameter 2 mm, length 15 mm) containing the sample. Due to the small volume of the sample (about 4 μL) and the thin glass walls (0.5 mm), the heat exchange is very efficient and leads to a high cooling rate. Under these conditions the disordered structure of the respective liquid solidifies. The sample tube is then transferred from the liquid nitrogen bath into a cryostat, which maintains the sample at 140 K in a cold nitrogen gas stream. The design of this cryostat has been described elsewhere.[28] The setup enables us to anneal the sample at temperatures between 140 K and the respective melting point at a rate of approximately 5 K min^{-1}.

The low-frequency Raman spectra have been recorded using a Dilor RTI30 spectrometer focusing an argon ion laser (514.5 nm) for excitation and permitting a power of 150 mW through the double-walled cryostat onto the capillary. The scattered light was collected perpendicular to the incident laser beam. Plasma

* Corresponding author. Tel: +43 1 25077 3809. Fax: +43 1 25077 3890. E-mail: grothe@tuwien.ac.at.
† Vienna University of Technology.
‡ University of Oslo.

10.1021/jp055521t CCC: $33.50
Published on Web 12/10/2005

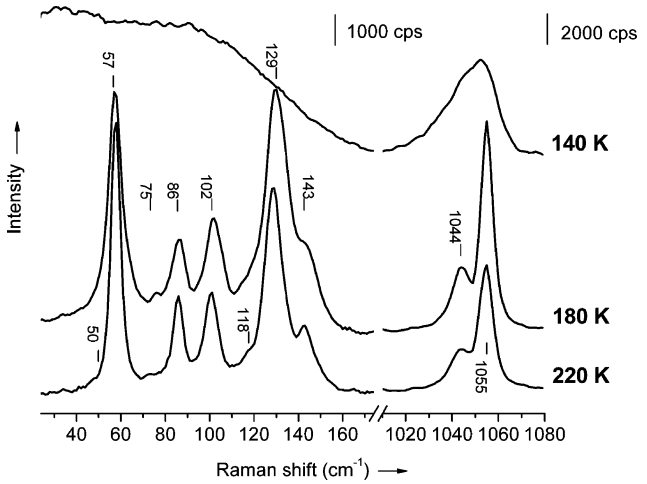

Figure 1. Raman spectra of 50 mol % HNO_3: (from top to bottom) samples are annealed at 140, 180, and 220 K and measured at these temperatures.

lines of the laser light were suppressed by the use of a filter, and both the Stokes and anti-Stokes spectra were recorded. The resolution of the Raman spectra was as a standard 3.5 cm^{-1}. For higher resolution the slit width was reduced to give a resolution of 2 cm^{-1}. The scattered light at every position of the grating has been accumulated for 4 s.

Survey spectra of the mid-frequency region have been recorded using a HORIBA Lab Ram spectrometer equipped with an Olympus BX microscope. A He−Ne laser was focused through the microscope onto a special designed cryostat mounted on the microscope table. For sample preparation, the quenching technique of Tizek et al. was applied.[25]

3. Results

We have studied the Raman spectra at temperatures from 140 K, which is 20 K below the average glass transition temperature of nitric acid hydrates, and up to the melting points. The crystallization of the hydrates $HNO_3.xH_2O$ ($x = 1-3, 5$) occurs between 150 and 170 K, depending on the stoichiometry of the sample and the quenching procedure. The crystallization process can be followed visually: the sample turns from transparent into opaque. In Figures 1−6, the Raman spectra document the annealing process of five different nitric acid mole fractions: $x_{HNO3} = 0.5$, 0.4, 0.33, 0.25, and 0.19. The topmost trace in the figures always shows the spectrum of the amorphous sample. The right-hand trace exhibits the broad symmetric NO_3 stretching vibration of the nitrate ion peaking between 1050 and 1054 cm^{-1}. At concentrations higher than $x_{HNO3} = 0.25$, the symmetric NO_2 stretching of undissociated HNO_3 at 1307 cm^{-1} gains intensity (not shown here) − the HNO_3 band subsequently disappears in the course of crystallization. In the low-frequency region no distinct bands are observable, and only a general scattering intensity increase can be recognized. However, this frequency range gains particular importance during the crystallization process when phonon bands grow in approving the formation of different crystal lattices. For the evaluation of this process five concentration are chosen (see above), at which the crystallization behavior and the phase composition have already been investigated in previous XRD studies.[25,29]

3.1. Concentration of 50 mol % HNO_3. The crystallization process of a 50 mol % HNO_3 solid is monitored in Figure 1. During the annealing from 140 to 180 K the broad symmetric NO_3^- stretching splits into two bands at 1044 and 1055 cm^{-1}, due to nonequivalent H_3O^+ groups. At the same time six bands grow up in the low-frequency region: the wavenumbers are collected in Table 1. The spectral pattern has two intense bands at 57 and 129 cm^{-1}; four bands of medium intensity at 75, 86, 102, and 143 cm^{-1}; and additionally two very small shoulders are hardly recognizable at 50 and 118 cm^{-1}. The pattern stays constant with respect to relative intensity during annealing up to 220 K; also, it does not change when re-cooling the sample to 140 K (not shown here). The pattern is in good agreement with the low-frequency Raman spectra of NAM recorded by Herzog-Cance et al.[4] The constancy of the relative intensity ratios with respect to temperature is in perfect agreement with the previously reported diffractograms.[25] Thus, it is evidenced that crystallization of NAM occurs and that this phase is stable until it melts at 235 K.

TABLE 1: Low-Frequency Raman Bands (cm^{-1}) of NAM, α-NAD, and β-NAD

NAM		α-NAD in a mixture with NAM		β-NAD in a mixture with NAM		β-NAD	
140 K	220 K	180 K[a]	180 K	220 K[a]	220 K	180 K	220K
		35	31 (s)				
				52	52 (w)	49	49 (w)
62	58 (s)[b]						
				71	76 (s)	76	76 (s)
77	75 (w)						
		85	81 (s)				
89	86 (m)	*c*	88 (w)	*c*	90 (w)	91	91 (w)
				94	95 (s)	96	97 (s)
105	101 (m)	101	98 (w)				
		114	113 (s)	*c*	114 (m)	113	114 (m)
121	118 (w)						
134	129 (s)			134	132 (m)	134	135 (m)
148	143 (m)						

[a] Re-cooled to 140 K. [b] Intensities: s (strong), m (medium), w (weak). [c] Overlapping with NAM-bands.

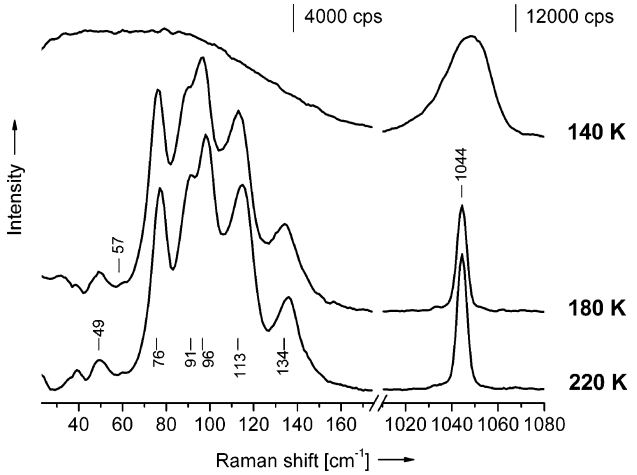

Figure 2. Raman spectra of 33.3 mol % HNO_3: (from top to bottom) samples are annealed at 140, 180, and 220 K and measured at these temperatures.

3.2. Concentration of 33.3 mol % HNO_3. From diffraction experiments it is known that pure β-NAD is the only phase crystallizing from amorphous 33.3 mol % HNO_3.[25] The respective Raman spectra of pure β-NAD are presented in Figure 2. In the low-frequency range six bands at 49, 76, 91, 96, 113, and 134 cm^{-1} (Table 1) are characteristic for β-NAD. At 33.3 mol % the β-NAD pattern appears unique and unperturbed, and the relative intensities change only slightly with temperature. Probably a small amount of NAM is present, recognized by the very weak signal of the distinct NAM band located at 57 cm^{-1}.

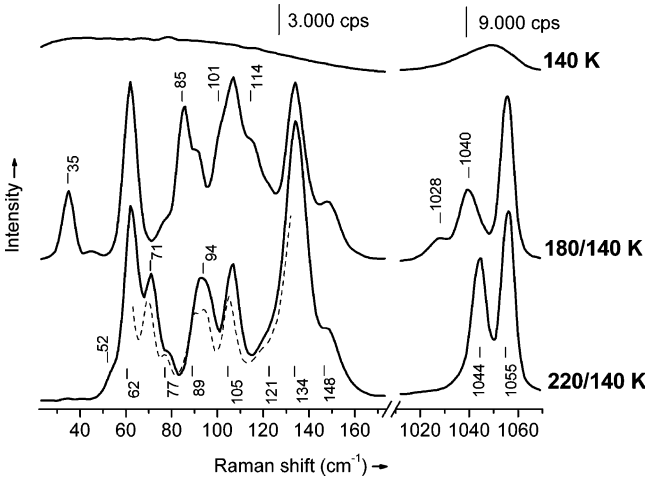

Figure 3. Raman spectra of 40 mol % HNO_3: (from top to bottom) samples are annealed at 140, 180, and 220 K but are re-cooled to 140 K before measurement; dashed line: same sample as at 220/140 K but with 2 cm^{-1} resolution.

3.3. Concentration of 40 mol % HNO_3. Figure 3 exhibits the spectral changes of a nonstoichiometric concentration, which forms a mixture of several hydrates of different composition upon annealing and, consequently, in a complicated spectrum with overlapping bands. After crystallization at 180 K three bands appear in the symmetric NO_3^- stretching region: 1028, 1040, and 1055 cm^{-1}. The most intense band at 1055 cm^{-1} and a weak shoulder — assumed at 1044 cm^{-1}—are assigned to NAM (see Figure 1). When annealing to 220 K only the band at 1055 cm^{-1} remains, while the bands at 1028 and 1040 cm^{-1} disappear and a new intense band at 1044 cm^{-1} grows in. The band positions at 220 K are essentially the same as in NAM (1044 and 1055 cm^{-1}, see Figure 1) — only the relative intensity is very different. The low-frequency region is more expressive: at 180 K nine bands appear. The strongest bands in the spectrum are recognized at 62 and 134 cm^{-1} and originate from NAM. In the region between these bands, a considerable overlap between NAM bands and a couple of new bands can be registered. Spectra recorded with higher spectral resolution (2 cm^{-1}) are shown in Figure 4a and evidence that there are six distinct bands (76, 81, 88, 98, 101, and 113 cm^{-1}) in this region. Four of these bands (81, 88, 98, and 113 cm^{-1}) clearly do not belong to the NAM pattern. In addition, a new and very remarkable band appears at 35 cm^{-1} (Figure 3, 180/140 K) — the same band is at 31 cm^{-1} at 180 K (not shown). All five new bands (31, 81, 88, 98 and 113 cm^{-1}) are assigned to α-NAD at 180 K.

In general, all NAM bands of Figure 3 are blue-shifted by about 2−5 cm^{-1}. This becomes clear when comparing the NAM bands in Figure 3 with those of the pure NAM spectrum (Figure 1). It has to be considered that the sample has been re-cooled after each annealing step down to 140 K before recording the spectra given in Figure 3. As all phase changes can be caused already by small temperature changes and are irreversible, this procedure has the advantage of preventing an uncontrolled heating and change of the sample by the laser during the measurement. Thus, at 180 K the sample yields already some traces of β-NAD (dashed line, Figure 4a).

After annealing to 220 K, the α-NAD bands disappear, the NAM bands remain constant, and three new features grow in at 52, 71, and 94 cm^{-1} (Figure 3). Again, at higher spectral resolution (dashed line), six bands (71, 77, 89, 94, 105, and 121 cm^{-1}) can be distinguished in the region between the strongest NAM bands at 62 and 134 cm^{-1}. Figure 4a shows the α-NAD bands disappearing (arrows down) and the β-NAD bands growing in (arrows up), but the spectrum is slightly different from the corresponding one in Figure 3. This is due to the varied temperature regime at which the sample was prepared and measured (see above). At 220 K, bands at 52, 76, 90, 95, and 114 cm^{-1} are assigned to β-NAD. However, the intensity ratio between the NAM bands at 62 and 134 cm^{-1} in Figure 3 is markedly changed compared to that of Figure 1 (pure NAM). An additional band is thus overlapping the NAM band at 134 cm^{-1} and is also assigned to β-NAD. Due to the overlap of the many bands in the region from 70 to 135 cm^{-1} originating from α-NAD, β-NAD, and NAM, the phase transition from α-NAD to β-NAD is best inspected by the disappearance of the α-NAD band at 35 cm^{-1} and the appearance of the β-NAD band at 71 cm^{-1} (Figure 3). In the mixture, the positions of both bands show remarkable temperature dependencies shifting, in the opposite direction, to 31 cm^{-1} at 180 K and 76 cm^{-1} at 220 K, respectively (see Table 1). The previously presented diffractogram from the same process ensures that a phase change occurs, transforming α-NAD into β-NAD while the amount of NAM remains constant.[25]

In Figure 4b, the spectra of pure NAM (50 mol %) and pure β-NAD (33 mol %) are stacked in line with the spectrum of the respective mixture (40 mol %). Comparing these spectra, it becomes obvious that the spectrum of the mixture can be retraced by a linear combination of the two pure hydrate spectra.

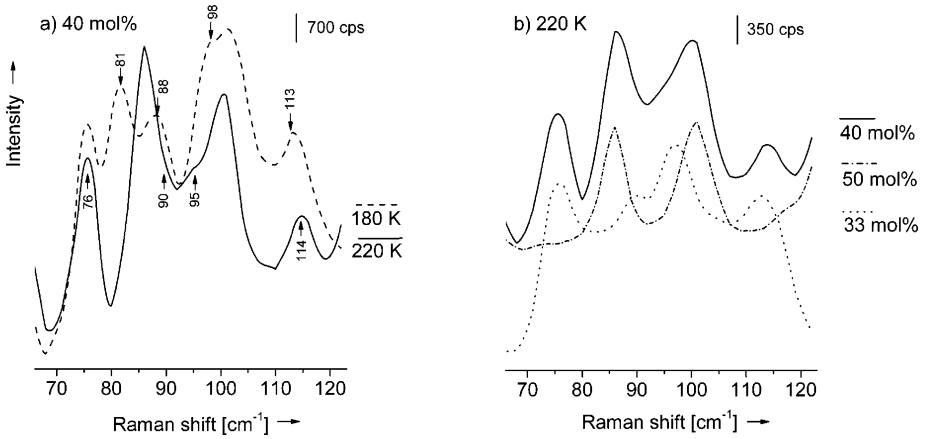

Figure 4. (a) Left side: Raman spectra of 40 mol % HNO_3 at 2 cm^{-1} resolution: dashed line 180 K, solid line 220 K. Arrows showing down designate α-NAD bands decreasing with temperature, and arrows showing up designate β-NAD bands increasing with temperature. (b) Right side: Raman spectra of three different concentrations at 220 K: solid line 40 mol %, dash-pointed line 50 mol %, short-dashed line 33.3 mol % HNO_3.

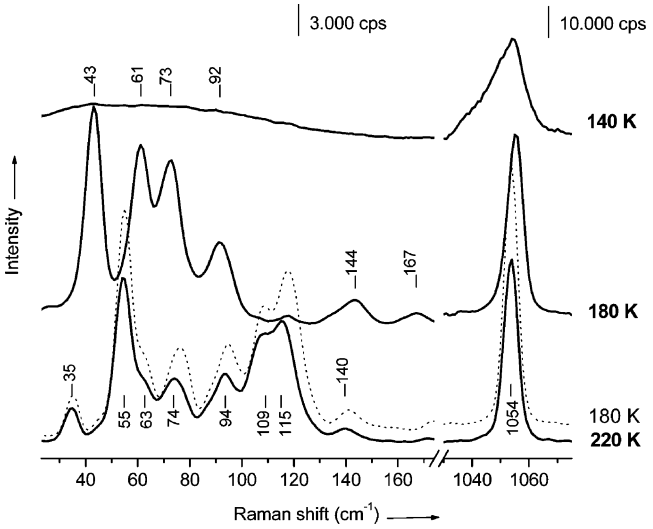

Figure 5. Raman spectra of 25 mol % HNO_3: (from top to bottom) samples are annealed at 140, 180, and 220 K and measured at these temperatures. Finally, the sample has been re-cooled to 180 K (dashed line) showing the phase change being irreversible.

3.4. Concentration of 25 mol % HNO_3. Figure 5 shows the spectra from annealing a 25 mol % HNO_3 sample which crystallizes below 170 K. A rather narrow band at 1056 cm^{-1} appears, and upon annealing from 180 to 220 K this band shifts only very slightly to 1054 cm^{-1}. In the low-frequency range, remarkable changes are observed in the same temperature interval. At 180 K, six bands (four intense bands at 43, 61, 73, and 92 cm^{-1} and two weak bands at 144 and 167 cm^{-1}) appear. These bands completely vanish at 220 K and are replaced by eight new bands — two strong bands at 55 and 115 cm^{-1} with shoulders at 63 and 109 cm^{-1} and four weak bands at 35, 74, 94, and 140 cm^{-1}. On re-cooling to 180 K these bands do not change their relative intensities, but the band positions are slightly shifted to higher wavenumbers. Diffraction experiments evidence an irreversible phase change from α- to β-NAT.[29]

3.5. Concentration of 19 mol % HNO_3. When changing the concentration down to 19 mol % HNO_3, the diffraction experiments of Tizek et al.[29] did not reveal pure α-NAT and ice as expected, but a new diffraction pattern which was tentatively assigned to the pentahydrate NAP in accordance with the early experiments of Marti and Mauersberger.[30] At temperatures above 175 K, NAP transforms irreversibly into β-NAT and ice. The Raman spectra (Figure 6) exhibit the same changes in the given temperature interval. After crystallization at 153 K, there are two bands in the NO stretch region at 1044 and 1054 cm^{-1} recorded here at 170 K. The former one disappears and the latter gains intensity by more than one order of magnitude upon annealing to 220 K. Since all nitric acid hydrates show the symmetric NO_3^- stretching in the same narrow interval, it is not obvious which of the known hydrates have crystallized or if even a new phase arose — at concentrations between 50 and 40 mol % the same two bands are always present at 1044 and 1055 cm^{-1} but with inverted intensity ratio, possibly caused by different cations next to the nitrate. However, the information collected from the low-frequency region is more clear exhibiting a pattern of six bands — one strong band at 50 cm^{-1} and five weaker bands at 66, 86, 107, 117, and 137 cm^{-1}. These bands disappear at temperatures above 175 K, and the well-known β-NAT pattern of eight bands observed in the 25 mol % spectra (see Figure 5) grows.

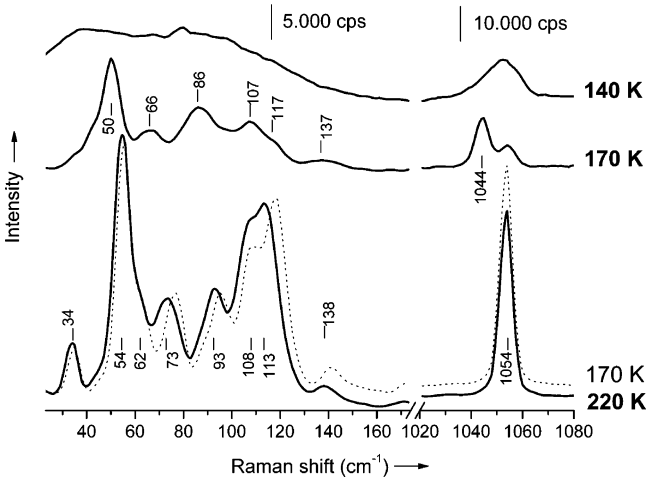

Figure 6. Raman spectra of 19 mol % HNO_3: (from top to bottom) samples are annealed at 140, 170, and 220 K and measured at these temperatures. Finally, the sample has been re-cooled to 170 K (dashed line) showing the phase change being irreversible.

4. Discussion

During the quenching procedure, thermodynamically unstable crystal germs are formed and embedded in the otherwise amorphous sample. In the annealing process some of these germs grow, and the most stable germs form the respective crystals. The amorphous sample exhibits broad bands (Figures 1−3, 5, 6; top trace, right side) reflecting the anisotropic environment of molecules and ions in the amorphous solid. In the low-frequency region, no distinct bands are observed since the amorphous state — the same as a solidified liquid — has a diffuse density of low-lying states. As soon as the crystallization process occurs, the symmetric stretching vibration of the nitrate ion changes its shape and position. It becomes narrower with a slightly different position at higher wavenumbers. In some cases (NAM, α-NAD, NAP — Figures 1, 2, 6) also a splitting is observed. However, all these changes are rather unspecific and could alternatively also result from distortions, defects, or orientations of the crystal.[21,23,31] To obtain spectroscopic information of comparable specificity with the diffraction data, the place to look is in the low-frequency region of the Raman spectrum, with its lattice vibrations intimately related to the symmetry and structure of the unit cell of the crystal. In general, crystal spectra exhibit bands from two types of vibration: (1) internal modes (intramolecular vibrations), and (2) external modes (intermolecular vibrations or lattice modes).

All nitric acid hydrates are built from the same ions and molecules: NO_3^-, H_2O, and specific ionic $H_{2n+1}O_n^+$ species ($n = 1-3$), which exhibit broad and overlapping bands in the mid-frequency region. To a first approximation, the Raman activity of the unperturbed species is given by the selection rules according to their symmetry. For the nitrate ion of D_{3h} symmetry there are three bands designated $\delta_{as}(E')$, $\nu_s(A_1)$, and $\nu_{as}(E')$; for water (C_{2v}) there are three bands $\delta(A_1)$, $\nu_s(A_1)$, and $\nu_{as}(B_1)$; for oxonium (C_{3v}) there are four bands $\delta_s(A_1)$, $\delta_{as}(E)$, $\nu_{as}(E)$, $\nu_s(A_1)$; and for aquaoxonium (C_2) there are even 15 bands. All of these bands are Raman active and exhibit very different intensities in the spectrum. Thus, several Raman active bands are too weak to be observed. The most intense band, however, is the symmetric NO_3^- stretching vibration, which has been monitored in the course of this work. Additional spectroscopic features are caused by the static field effect, which lowers the symmetry of the ions and molecules at a particular lattice site. This effect may produce: shifts in frequencies, splitting of

degenerated fundamentals, appearance of "forbidden" fundamentals, and coupling of molecules within the unit cell (correlation field effect). Anyhow, these effects are of little help in differentiating between the particular phases. A detailed assignment assisted by a factor group analysis, which takes into account the space group, the number of molecules and atoms per unit cell, and the site symmetries, could be elucidative. However, even a complete assignment of all bands in the mid-frequency region would not ensure a phase differentiation.

The low-frequency region is more suited for the spectroscopic phase analysis, since it exhibits additional bands resulting from the crystal lattice. The unit cell of a hydrate contains a certain number of nitrate, oxonium, and water molecules, which are interconnected by hydrogen bonds forming networks of different structure. The intermolecular vibrations of these structures involve the relative motions of the molecules or ions as a whole within the crystal lattice. For a unit cell with P molecules there are $3(2P - 1)$ intermolecular vibrations, of which $3(P - 1)$ are translational modes and $3P$ are librational modes (hindered rotation).[32] Water ice, clathrates, and hydrates exhibit similar low-frequency Raman spectra,[33,34] their librational modes (wagging, rocking, and twisting modes) are peaking in the region 300−650 cm^{-1}.[33] Further rotational and translational modes of these compounds are usually situated below 300 cm^{-1}. Water ice shows vibrations of disordered hydrogen bonds between 250 and 300 cm^{-1}.[36] Distinctive hydrogen bonds can be correlated with translational modes below 250 cm^{-1}. Water ice shows a stretching mode at 210 cm^{-1} and a deformation mode at 60 cm^{-1}.[37] Nitric acid hydrates include ions with higher reduced masses but similar force constants, and thus, shift the vibrations to lower wavenumbers (about −30%).

The only calculations of low-frequency vibrations of nitric acid hydrates have been performed by Escribano et al.[24] However, these calculations are based on uncharged clusters of HNO_3 and H_2O and therefore are not comparable with ionic solids. For the correct assignment of all lattice vibrations, again, only the factor group analysis would help. However, in primitive space groups, such as in the present cases, most intermolecular modes are Raman active. Due to their high number they are extremely difficult to discriminate. Therefore, we use a model approach by considering two molecules or molecular ions connected by a strong hydrogen bond as a local structure, the intermolecular vibrations of which are adopted as essentially independent of the rest of the respective unit cell. This simplified model predicts six characteristic vibrations: $[3(Q_1 + Q_2) - 6]_{complex} - [(3Q_1 - 6) + (3Q_2 - 6)]_{isol.\ molec.} = 6$, where Q_1 and Q_2 are the numbers of atoms in the respective molecules. Two of these complex bands should have remarkable intensities in the Raman spectrum. Namely, an intermolecular stretch and an intermolecular bending mode of every hydrogen bond can be assigned. Taking into account all strong hydrogen bonds of the respective crystal, the Raman pattern in the region between 20 and 180 cm^{-1} can be explained to a first approximation.

NAM has an orthorhombic structure,[38] which contains four nitrates and four oxonium ions per unit cell with space group $P2_1cn$ (C_{2v}^9). There are 21 translational and 24 librational modes, which in principle are all Raman active. In NAM, all HNO_3 and H_2O molecules are completely dissociated into NO_3^- and H_3O^+, respectively. Every H_3O^+ is connected with three NO_3^- forming parallel layers. In the whole structure there are three different kinds of hydrogen bonds. Every hydrogen bond has six independent vibrations adding up to 18 intermolecular modes. However, for every hydrogen bond there should be at least two intense bands, one stretch and one deformation mode of $NO_3^-\cdots H_3O^+$. This corresponds to the six bands registered in the spectrum (Figure 1). Further 12 bands, in principle, are also Raman active but have much lower intensities and thus contribute to the underground of the low-frequency region.

Both modifications of NAD have a monoclinic structure and space group $P2_1/n$ (C_{2h}^2) containing eight nitrates and eight aquaoxonium ions per unit cell.[38,39] Every nitrate connects two oxonium groups, which are in a junction with a water molecule each. These structural units ($NO_3^-\cdots H_5O_2^+$) are interconnected as endless planar layers. In the low-temperature modification always two of these layers are mirror-symmetrically linked by weak O···H interactions. In the high-temperature modification the same layers are formed but are interconnected three-dimensionally through water molecules. Both phases have 45 translational and 48 librational modes. There are seven different hydrogen bonds per unit cell, but only three rather strong hydrogen bridges, which form the layers. Therefore, instead of 14 bands, only six bands should gain considerable intensity. For β-NAD exactly these six bands have been found (Figure 2), but in the case of α-NAD the situation is puzzling since it has never been crystallized as a pure phase. Only four bands have been identified unambiguously — two missing bands are probably hidden by NAM and/or β-NAD bands (Figure 3).

In the case of NAT, the crystal structure has only been solved for the high-temperature modification. β-NAT has space group $P2_12_12_1$ (D_2^4) with four nitrate and four diaquaoxonium ions per unit cell,[38] which leads to 21 translational and 24 librational modes. Each H_3O^+ ion is connected with two water molecules forming the $H_7O_3^+$ unit. The diaquaoxonium elements are interconnected by weak hydrogen bonds into a helix. The nitrate ions are embedded in this spiral by strong hydrogen bridges. In this way, layers are constructed forming a three-dimensional network. In the spectrum, six strong- or medium-intensity bands can be recognized in the region between 50 and 120 cm^{-1} (Figure 5, 220 K). These are probably related to the bridges, which embed the nitrate ions. Below 40 cm^{-1} there is only one band, which could be due to the weak interactions inside the helix.

For α-NAT and NAP, the crystal structures have not yet been solved. Therefore, a detailed analysis of the spectra is not attempted here. However, in the case of α-NAT we have concluded from the mid-infrared spectra that there are two different kinds of hydrate water.[29] Unlike β-NAT, the diaquaoxonium ion does not emerge as a recognizable structural element. The water molecules are arranged in different distances to the oxonium groups and could also be viewed as guest-molecules inside the lattice. Thus, the intense band at 43 cm^{-1} (Figure 5, 180 K) is tentatively attributed to these water molecules.

In general, the positions of all phonon bands are rather sensitive to temperature and concentration. Two general trends can be concluded for all hydrate bands in the low-frequency region:

(a) With increasing temperature the crystal lattice expands and the respective lattice vibrations are all red-shifted.

(b) Concentration changes result in crystal mixtures with coexisting hydrates or ice. The foreign elements or units may cause mechanical stress on the crystals under investigation. The lattice vibrations then show nonuniform shifts depending on the particular situation of every crystal mode.

Apart from the above-mentioned band position's dependencies, the relative intensities of the bands remain constant. Therewith, the overall pattern of a low-frequency Raman spectrum can be considered as a kind of fingerprint of a

particular hydrate, which can be added, subtracted, or shifted for phase assignment.

5. Conclusion

This is the first time that low-frequency Raman spectra of the polymorphs of nitric acid hydrates are recorded and mixtures of different hydrates are resolved. Altogether, six different phases and the same number of phase changes are investigated, two of which are transitions from a low- to a high-temperature modification. The relation between the structure and the low-frequency spectra is discussed. The spectra correlate rather well with the differences in the networks of hydrogen bonds, which are the framework of the particular hydrate structures. Every intermolecular vibration, as a first approximation, is understood as the motion of an ion and/or molecule in relation with these interactions. Therefore, every hydrogen bond has been considered as a kind of bimolecular complex, which causes at least two additional bands in the low-frequency region. These bands sum up to a fingerprint of the particular structure, and differences of these patterns were applied in order to assign the spectra of hydrate mixtures.

The information content of low-frequency Raman spectroscopy is comparable to that of terahertz absorption spectroscopy, which is very applicable for the estimation of the phase composition of solid samples. However, Raman spectra exhibit narrower bands than far-infrared spectra, and therefore are more suitable for the differentiation of band patterns. The knowledge of the phonon band may particularly help in Raman microscope studies where the nucleation of acid droplets can be observed in situ.[11] Within such a nucleation process, coexisting phases can be differentiated and their appearance and disappearance can be followed over the time. Here low-frequency spectroscopy gives an additional advantage against diffraction techniques by being less time-consuming and more specific to nano-crystallinity (nano-crystals are below the detection limit of XRD). This opens up a possible pathway for the investigation of crystal nuclei and their growth. Thus, the transition from the liquid to the solid phase and from metastable to stable modifications could be investigated in more detail by the use of a Raman microscope. Therefore, it will be especially helpful to know the low-frequency spectra of all pure hydrates in the respective phase diagram, thus, exhibiting fundamental differences in the low-frequency region, which appear to be much more relevant than the unspecific changes of the mid-frequency region.

Acknowledgment. The present work was funded through the Hochschuljubiläumsstiftung der Stadt Wien, project H-1119, Vienna University of Technology, innovative project 2003, and the Austrian Exchange Service (OAD). H.G. acknowledges a stipend from the University of Oslo, program for international cooperation, and from the Vienna University of Technology, Ausseninstitut. Thanks are due to Prof. Peter Klaeboe for support and helpful discussion.

References and Notes

(1) Pickering, S. U. *J. Chem. Soc.* **1893**, *63*, 436−443.
(2) Luzzati, V. *Acta Crystallogr.* **1951**, *4*, 120−131.
(3) Luzzati, V. *Acta Crystallogr.* **1953**, *6*, 152−164.
(4) *Proceedings of the International Conference on Raman Spectroscopy.*, 6th ed.; Schmid, E. D., Krishnan, R. S., Kiefer, W., Eds.; Heyden: London, 1978; Volume 2, 276−277.
(5) Herzog-Cance, M. H.; Potier, J.; Potier, A.; Dhamelincourt, P.; Sombret, B.; Wallort, F. *Adv. Mol. Relax. Interaction Processes* **1979**, *15*, 1−23.
(6) Solomon, S.; Garcia, R. R.; Rowland, F. S.; Wuebbles, D. J. *Nature* **1986**, *347* (6291), 347−354.
(7) Tabazadeh, A.; Djikaev, Y. S.; Hamill, P.; Reiss, H. *J. Phys. Chem. A* **2002**, *106*, 10238−10246.
(8) Tolbert, M. A.; Toon, O. B. *Science* **2001**, *292* (5514), 61−62.
(9) Zondlo, M. A.; Hudson, P. K.; Prenni, A. J.; Tolbert, M. A. *Annu. Rev. Phys. Chem.* **2000**, *51*, 473−499.
(10) Fahey, D. W.; Gao, R. S.; Carslaw, K. S.; Kettleborough, J.; Popp, P. J.; Northway, M. J.; Holecek, J. C.; Ciciora, S. C.; McLaughlin, R. J.; Thompson, T. L.; Winkler, R. H.; Baumgardner, D. G.; Gandrud, B.; Wennberg, P. O.; Dhaniyala, S.; McKinney, K.; Peter, T.; Salawitch, R. J.; Bui, T. P.; Elkins, J. W.; Webster, C. R.; Atlas, E. L.; Jost, H.; Wilson, J. C.; Herman, R. L.; Kleinbohl, A.; von Konig, M. *Science* **2001**, *291* (5506), 1026−1031.
(11) Knopf, D. A.; Koop, T.; Luo, B. P.; Weers, U. G.; Peter, T. *Atmos. Chem. Phys.* **2002**, *2*, 207−214.
(12) Tabazadeh, A.; Jensen, E. J.; Toon, B.; Drdla, K.; Schoebert, M. R. *Science* **2001**, *291* (5513), 2591−2594.
(13) Tabazadeh, A.; Santee, M. L.; Danilin, M. Y.; Pumphrey, H. C.; Newman, P. A.; Hamill, P. J.; Mergenthaler, J. L. *Science* **2000**, *288* (5470), 1407−1411.
(14) Worsnop, D. R.; Fox, L. E.; Zahniser, M. S.; Wofsy, S. C. *Science* **1993**, *259*, 71−74.
(15) Ritzhaupt, G.; Devlin, J. P. *J. Phys. Chem.* **1991**, *95*, 90−95.
(16) Barton, N.; Rowland, B.; Devlin, J. P. *J. Phys. Chem.* **1993**, *97*, 5848−5851.
(17) Middlebrook, A. M.; Berland, B. S.; George, S. M.; Tolbert, M. A.; Toon, O. B. *J. Geophys. Res.* **1994**, *99* (D12), 25655−25666.
(18) Koehler, B. G.; Middlebrook, A. M.; Tolbert, M. A. *J. Geophys. Res.* **1992**, *97*, 8067−8074.
(19) Peil, S.; Seisel, S.; Schrems, O. *J. Mol. Struct.* **1995**, *348*, 449−452.
(20) Koch, T. G.; Holmes, N. S.; Roddis, T. B.; Sodeau, J. R. *J. Phys. Chem.* **1996**, *100*, 11402−11407.
(21) Koch, T. G.; Holmes, N. S.; Roddis, T. B.; Sodeau, J. R. *J. Chem. Soc., Faraday Trans.* **1996**, *92* (23), 4787−4792.
(22) Bertram, A. K.; Sloan, J. J. *J. Geophys. Res.* **1998**, *103* (D3), 3553−3561.
(23) Tisdale, R. T.; Prenni, A. J.; Iraci, L. T.; Tolbert, M. A.; Toon, O. B. *Geophys. Res. Lett.* **1999**, *26*, 707−710.
(24) Escribano, R.; Couceiro, M.; Gomez, P. C.; Carrasco, E.; Moreno, M. A.; Herrero, V. J. *J. Phys. Chem. A* **2003**, *107*, 651−661.
(25) Tizek, H.; Knözinger, E.; Grothe, H. *Phys. Chem. Chem. Phys.* **2002**, *4*, 5128−5134.
(26) Grothe, H.; Myhre, C. E. L.; Tizek, H. *Vibr. Spectrosc.* **2004**, *34*, 55−62.
(27) Lebrun, N.; Mahe, F.; Foulon, M.; Gors, C.; Petit, J. C. *Can. J. Phys.* **2003**, *81*, 61−69.
(28) Miller, F. A.; Harney, B. M. *Appl. Spectrosc.* **1970**, *24*, 291−292.
(29) Tizek, H.; Knözinger, E.; Grothe, H. *Phys. Chem. Chem. Phys.* **2004**, *6*, 972−979.
(30) Marti, J. J.; Mauersberger, K. *J. Phys. Chem.* **1994**, *98*, 6897−6899.
(31) Maté, B.; Ortega, I. K.; Moreno, M. A.; Escribano, R.; Herrero, V. J. *Phys. Chem. Chem. Phys.* **2004**, *6*, 4047−4055.
(32) Finch, A.; Gates, P. N.; Radcliffe, K.; Dickson, F. N.; Bentley, F. F. In *Chemical Applications of Far Infrared Spectroscopy*; Academic Press: London, 1970.
(33) Takasu, Y.; Nishio, I. *J. Phys. Soc. Jpn.* **2003**, *72* (8), 2106−2109.
(34) Tomikawa, K.; Kanno, H. *J. Phys. Chem. A* **1998**, *102*, 6082−6088.
(35) Piszczek, P.; Grodzichki, A.; Engelen, B. *J. Mol. Struct.* **2003**, *646*, 45−54.
(36) Li, J.; Ross, D. K. *Nature* **1993**, *364*, 327.
(37) Takasu, Y.; Katsutoshi, I.; Nishio, I. *J. Phys. Soc. Jpn.* **2003**, *72* (5), 1287−1291.
(38) Lebrun, N.; Mahe, F.; Lamiot, J.; Petit, J. C.; Prevost, D. *Acta Crystallogr.* **2001**, *B57*, 27.
(39) Lebrun, N.; Mahe, F.; Lamiot, J.; Petit, J. C. *Acta Crystallogr.* **2001**, *C57*, 1129.